VIII. PLASMA MAGNETOHYDRODYNAMICS AND ENERGY CONVERSION*

Prof. G. A. Brown
Prof. E. N. Carabateas
Prof. S. I. Freedman
Prof. W. H. Heiser
Prof. M. A. Hoffman
Prof. W. D. Jackson
Prof. J. L. Kerrebrock
Prof. J. R. Melcher
Prof. J. P. Penhune
Prof. A. H. Shapiro
Prof. R. E. Stickney
Prof. H. H. Woodson
M. T. Badrawi
A. N. Chandra
R. S. Cooper
J. M. Crowley
D. A. East
J. R. Ellis, Jr.
J. Gerstmann
N. Gothard
J. B. Heywood
H. D. Jordan
P. G. Katona
F. D. Ketterer
G. B. Kliman
H. C. Koons
M. F. Koskinen
R. F. Lercari
W. H. Levison
A. T. Lewis
H. C. McClees, Jr.
C. W. Marble
T. D. Masek
J. T. Musselwhite
S. A. Okereke
J. H. Olsen
C. R. Phipps, Jr.
E. S. Pierson
D. H. Pruslin
M. H. Reid
C. W. Rook, Jr.
A. W. Rowe
M. R. Sarraquigne
M. Shroff
P. M. Spira
R. Toschi
G. L. Wilson
J. C. Wissmiller
B. M. Zuckerman

A. THERMIONIC EMISSION FROM MONOCRYSTALLINE TUNGSTEN SURFACES IN THE PRESENCE OF CESIUM

1. Introduction

The preliminary results of a recently initiated thermionic investigation are reported here, together with a brief description of our apparatus. The primary purpose of this study is to attain a better fundamental understanding of the emission processes that occur at the electrodes of thermionic energy converters.

A well-defined emitter surface is necessary in order to obtain experimental results of the quality that is most useful in the formulation of a general theory of thermionic processes. Monocrystalline surfaces are generally accepted as being the best specimens for such studies, and many investigators have employed them with varying degrees of success. Two of the most significant experiments are those of Nichols[1] and Smith,[2] the results of which show that the work function of clean tungsten depends markedly on the crystallographic structure of the particular surface that is being studied. The close-packed surfaces generally have the higher work functions, the approximate range for tungsten being from 4.65 ev down to 4.30 ev.

Although much work has been devoted to the study of clean monycrystalline surfaces, there have been very few quantitative investigations of monocrystalline surfaces that are partially covered with a layer of adsorbed molecules, a problem of current importance to thermionic energy conversion and ion propulsion. Qualitative observations have been made by a number of investigators,[3,4] and Webster[5] has obtained significant

*This work was supported in part by the National Science Foundation under Grant G-24073, and in part by the U.S. Air Force (Aeronautical Systems Division) under Contract AF33(616)-7624 with the Aeronautical Accessories Laboratory, Wright-Patterson Air Force Base, Ohio.

quantitative results for a few of the most conspicuous crystallographic directions of several refractory metals. The results show that cesium affects the close-packed planes most strongly, causing their work functions to be reduced by as much as 3 ev.

There is a definite need for additional research in this area since the existing theories are incomplete, and the experimental results are insufficient. For this reason, the present investigation has been designed to study in detail the dependence of the thermionic properties of tungsten on crystallographic direction, surface temperature, and cesium density.

2. Apparatus

An experimental tube built by Salomon[6] was modified for the present investigation. The design is basically a simplification of that used by Nichols.[1] The test specimen is a tungsten filament having a diameter of 0.0049 inch and a length of 14 cm. A long crystal has been grown in this filament by means of a special heating schedule.[4] Crystals formed in this manner are usually oriented in such a manner that the (110) crystallographic direction is parallel to the axis of the wire; this means that all crystallographic directions that are normal to the surface of the filament will have Miller indices of the form (hhk). Martin[3] has shown that this class of directions includes those of maximum and minimum emission; therefore it is most desirable for thermionic studies.

The filament is surrounded by a three-piece cylindrical anode (Fig. VIII-1). The two endpieces are fixed and serve as guard rings, while the center section is rotatable (by means of magnets) and contains a small slit cut parallel to the axis of the filament. The diameter of the center section is 1.9 cm, and the slit dimensions are 0.07 cm by 1.01 cm, so that the subtended angle is approximately 4.23°. By applying a strong electric field between the filament and the three-piece anode, one can cause the electrons emitted from the surface to be accelerated radially in straight-line paths. The slit acts as a microscope focused on a small area of the emitting surface, thereby allowing only the electrons from that area to pass through the slit to be measured at the collector. (The approximate value of this area for the present tube is 4.65×10^{-4} cm^2 if the filament-anode concentricity is perfect.) It is therefore possible, at least in principle, to measure the emission associated with the different crystallographic directions by rotating the slit to the appropriate positions.

A schematic of the electrical circuit is included in Fig. VIII-1. A dc power supply is used to maintain the three-piece anode at a potential of +1000 volts with respect to the filament. The cylindrical collector is held at potential of only 10 volts above that of the filament to reduce the undesirable effects of secondary emission. The collector current is measured with a suitable electrometer.

A cesium reservoir is connected to the experimental tube, and its temperature is regulated in order to attain the desired density of the cesium vapor. The tungsten

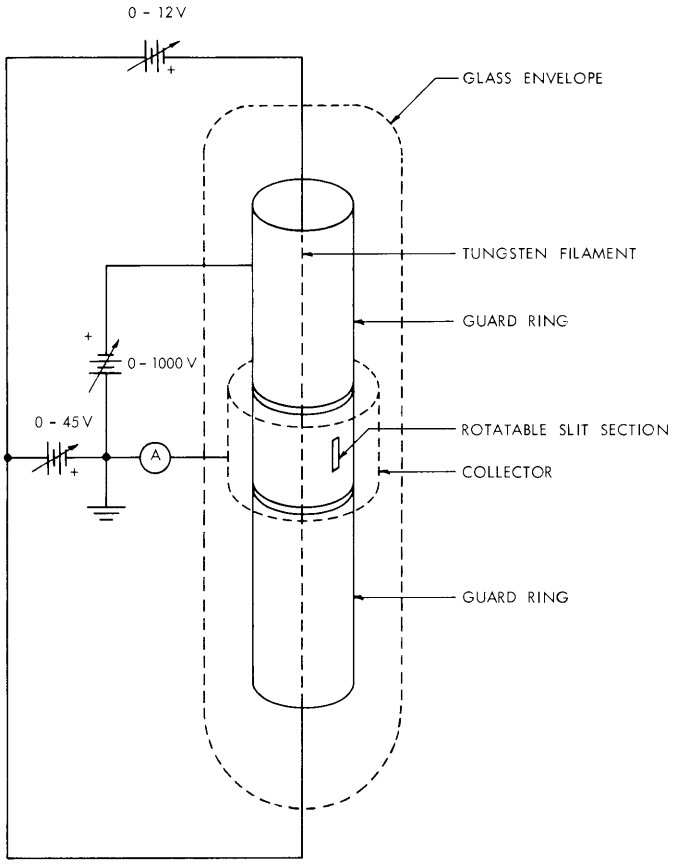

Fig. VIII-1. Experimental apparatus.

filament is heated directly by ac current, and its temperature is determined simply from the resistivity, a method that is of questionable accuracy at temperatures less than 1300°K unless the appropriate calibrations and corrections are made.[1]

3. Results

The tube was evacuated by means of a mercury diffusion-pump system, and a pressure of approximately 10^{-10} mm Hg was attained after thorough out-gassing. The filament was flashed a number of times until the emission pattern appeared to be stable. The filament temperature was then set at 1610°K, and readings of the collector current were taken for various slit positions. A portion of the data is shown in Fig. VIII-2, and its general pattern is similar to those reported by Nichols[1] and Smith.[2] Therefore, by referring to their work it was possible to estimate the positions of the prominent crystallographic directions along the abscissa. The abscissa actually represents the angular position of the slit; the pattern in Fig. VIII-2 does not cover the full 360° of azimuth, as its scope was limited to approximately 210°.

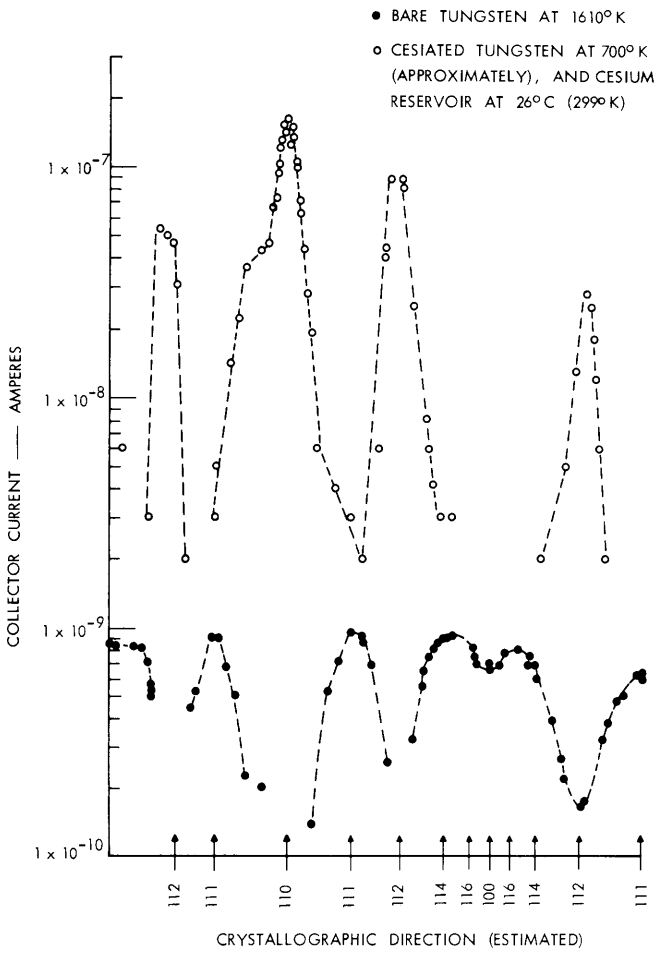

Fig. VIII-2. Thermionic emission vs crystallographic direction for cesiated and bare tungsten.

The tube was then sealed off from the vacuum system, and cesium was introduced by the usual method, that is, breaking a cesium-filled glass capsule in the reservoir. With the cesium reservoir at room temperature (26°C), the filament temperature was so adjusted as to obtain maximum emission in the (110) direction. (This temperature is not known accurately because a detailed calibration has not yet been performed; the estimated value is 700°K.) The resulting emission data for various slit positions are included in Fig. VIII-2 for comparison with the previous data obtained for bare tungsten. Since these are preliminary results, a detailed analysis is not warranted at this time. However, it is interesting to note that:

(i) The presence of cesium causes the maximum emission at 700°K to be as much as two orders of magnitude greater than that for the bare surface at 1610°K.

(ii) Surfaces having the lowest work function in the presence of cesium are those that have the highest "bare" work function.

Both of these general observations are in agreement with the results obtained by

other investigators.[3-5] On the basis of these preliminary results, we conclude that the present technique may be employed now in a more detailed study of emission processes.

4. Future Plans

The filament failed before more reproducible data could be obtained. A new filament is being prepared, and modifications have been made to reduce the effects of stray currents caused by leakage, secondary electrons, and photoemission. The immediate plan is to obtain data for other conditions of emitter temperature and cesium density.

The close cooperation of the members of the Physical Electronics Group of the Research Laboratory of Electronics has been invaluable throughout this program.

R. E. Stickney

References

1. M. H. Nichols, The thermionic constants of tungsten as a function of crystallographic direction, Phys. Rev. 57, 297 (1940).

2. G. F. Smith, Thermionic and surface properties of tungsten crystals, Phys. Rev. 94, 295 (1954).

3. S. T. Martin, On the thermionic and adsorptive properties of the surfaces of a tungsten single crystal, Phys. Rev. 56, 947 (1939).

4. G. G. Zipfel, S.B. Thesis, Department of Mechanical Engineering, M.I.T., 1960.

5. H. F. Webster, Thermionic emission from a tantalum crystal in cesium or rubidium vapor, J. Appl. Phys. 32, 1802 (1961).

6. S. N. Salomon, S.B. Thesis, Department of Mechanical Engineering, M.I.T., 1961.

B. A-C POWER GENERATION WITH MAGNETOHYDRODYNAMIC CONDUCTION MACHINES

Magnetohydrodynamic (MHD) power generation is attractive because of the inherent simplicity of the system. When an ionized gas is used as the working fluid, higher temperature operation is possible with an MHD generator. This makes heat rejection easier in space applications and increases thermal efficiency in ground-based installations.

In many applications, especially those in which the power is to be processed, it is desirable to generate ac power. Direct generation of ac power in MHD machines with ionized gases used as the working fluids has been studied extensively.[1] The several theoretical possibilities proposed thus far have been shown to be impractical for operation with conditions that are characteristic of combustion temperatures, either because electrical conductivity of the gas is too low or because too much external capacitance is necessary to provide the reactive power to excite the magnetic field.[1]

In this report we describe a new type of ac MHD power generator. It is a conduction

machine, and all reactive power is handled by inductive energy storages. Moreover, the criterion for successful operation as a self-excited ac machine is simply that the machine be suitable for self-excitation as a dc machine.

Although the system is most promising for application to gaseous MHD systems, the fundamental mechanism of operation will be demonstrated theoretically with an incompressible fluid mode. This is standard practice with many types of MHD conversion devices. After the system has been analyzed with scalar conductivity assumed, a configuration will be presented which is suitable for gases exhibiting a large Hall effect. Finally, some estimates of performance will be made for gas properties that are characteristic of temperatures at which gases can be contained by material walls.

1. System with Scalar Conductivity

Consider the system illustrated in Fig. VIII-3. It consists of a channel of constant cross-section area having the dimensions shown. An incompressible fluid flows with the velocity $\overline{v}$ in the direction shown. There are two pairs of electrodes feeding, through two sets of coils, two identical load resistances R_L. The generators formed by the two pairs of electrodes are assumed to be independent insofar as the fluid is concerned. That is, end and edge effects are neglected and the two circuits are electrically insulated

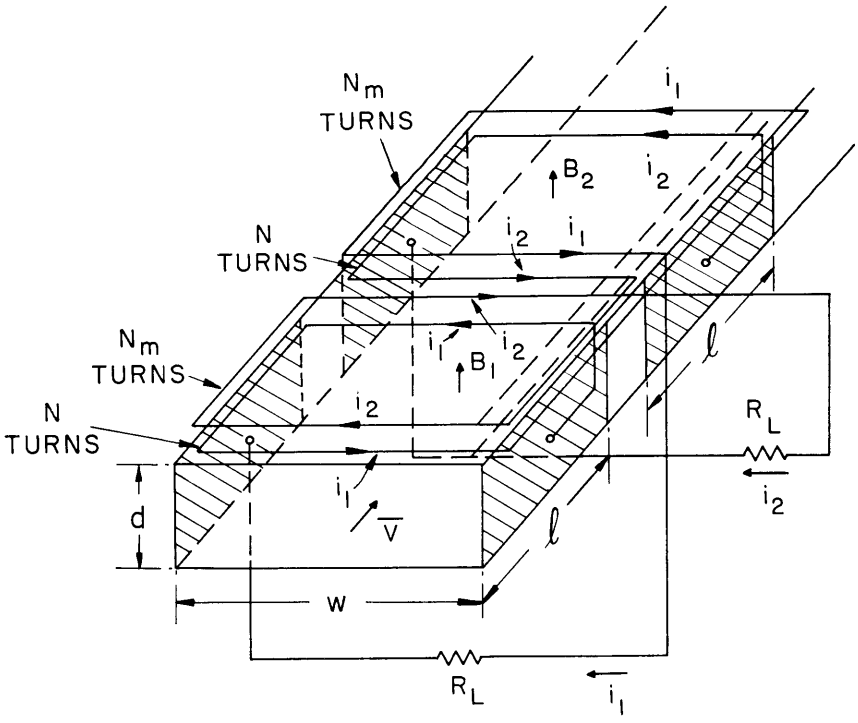

Fig. VIII-3. Basic configuration with solid electrodes.

from each other. Each of the two generators has two magnet coils, one carrying current i_1 and the other carrying current i_2 in the directions indicated. In practice, each coil would have a second half under the channel with the two connected series-aiding. Only one-half of each coil is shown in Fig. VIII-3 for simplicity. Although only two sets of electrodes and coils are shown, the system can have any number of sets. Furthermore, the sets can be connected for two-phase operation as in Fig. VIII-3 or for operation with any number of phases. In the last case, the number of coils associated with each pair of electrodes must be increased, but the essential features of ac operation are the same as those described below.

Denoting the magnetic flux density B_1 and B_2 in the regions of the two electrodes, assuming the positive directions shown in Fig. VIII-3, assuming the coils to be distributed so that the flux densities are essentially uniform over the length ℓ, and assuming that the coils produce a field just as a long solenoid (or assuming infinitely permeable pole pieces), we can write

$$B_1 = \frac{N\mu_o}{d} i_1 - \frac{N_m \mu_o}{d} i_2 \tag{1}$$

$$B_2 = \frac{N\mu_o}{d} i_2 + \frac{N_m \mu_o}{d} i_1 . \tag{2}$$

If we define the internal resistance for one pair of electrodes as

$$R_i = \frac{w}{\ell d \sigma} , \tag{3}$$

where σ is the electrical conductivity of the fluid, we can write the equations for the two circuits as

$$vwB_1 = Ri_1 + N\ell w \frac{dB_1}{dt} + N_m \ell w \frac{dB_2}{dt} \tag{4}$$

$$vwB_2 = Ri_2 + N\ell w \frac{dB_2}{dt} - N_m \ell w \frac{dB_1}{dt} . \tag{5}$$

Here, R is the total series resistance in one circuit ($R = R_L + R_i + R_c$, where R_c is the resistance of the magnet coils).

Substituting Eqs. 1 and 2 in Eqs. 4 and 5 and simplifying yields

$$Gi_1 - G_m i_2 = Ri_1 + L \frac{di_1}{dt} \tag{6}$$

$$Gi_2 + G_m i_1 = Ri_2 + L \frac{di_2}{dt} , \tag{7}$$

in which the parameters G, G_m, and L are defined as

$$G = \frac{vw\mu_o N}{d} \tag{8}$$

$$G_m = \frac{vw\mu_o N_m}{d} \tag{9}$$

$$L = \frac{\mu_o \ell w}{d}\left(N^2+N_m^2\right). \tag{10}$$

Elimination of i_2 from Eqs. 6 and 7, after some simplification, yields

$$\frac{d^2 i_1}{dt^2} + \frac{2(R-G)}{L}\frac{di_1}{dt} + \left[\frac{G_m^2 + (R-G)^2}{L^2}\right] i_1 = 0. \tag{11}$$

This equation has solutions of the form

$$i_1 = I_o \exp\left(-\frac{(R-G)}{L}t\right)\cos\left(\frac{G_m}{L}t + \theta\right), \tag{12}$$

where I_o and θ are constants to be evaluated from initial conditions. It is clear from the form of this solution that when $R > G$ the response is a damped sinusoid, when $R < G$ the response is an exponentially growing sinusoid, and when

$$R = G \tag{13}$$

the response is a sinusoid of constant amplitude. Reference to Eqs. 6 and 7 shows that Eq. 13 is the condition for self-excited operation as a dc generator.

Henceforth we shall assume that Eq. 13 is satisfied, in which case Eqs. 6 and 7 can be written

$$-G_m i_2 = L\frac{di_1}{dt} \tag{14}$$

$$G_m i_1 = L\frac{di_2}{dt}. \tag{15}$$

These equations, used with Eq. 12, show that i_1 and i_2 form a two-phase set. That is, if

$$i_1 = I_o \cos(\omega_m t+\theta), \tag{16}$$

Eq. 14 shows that

$$i_2 = I_o \sin(\omega_m t+\theta). \tag{17}$$

With the system parameters adjusted to satisfy Eq. 13, the system operates in the steady state with frequency

$$\omega = \frac{G_m}{L} \tag{18}$$

and with currents of finite amplitude. Consequently, power is dissipated in R_L and useful ac power is generated.

Equation 13 is the condition that must be satisfied for self-excitation as a dc generator with N turns on the field winding, and a coil resistance R_c in series with the load. The addition of the coupling windings N_m has transformed this pair of self-excited dc generators into a two-phase, self-excited ac generator. The price for making the change to ac operation is the addition of the N_m-turn coils that occupy space and contribute to resistance R_c. Reactive power is handled completely by the two magnetic storages having flux densities B_1 and B_2. Note that the two currents have 90° phase difference. The use of these currents in Eqs. 1 and 2 shows that B_1 and B_2 also have 90° phase difference. Thus the magnetic energy is constant in magnitude and oscillates between the two magnetic-field storages.

2. Limiting Parameters

Assuming steady-state ac operation, we can use the one-dimensional model in the analysis above to identify some limiting parameters of the system.

The use of Eqs. 9 and 10 in Eq. 18 yields

$$\omega = \frac{vN_m}{\ell\left(N^2+N_m^2\right)} . \tag{19}$$

It will be desirable to operate such a machine at as high a frequency as possible. With fixed v and ℓ, Eq. 19 has a maximum value when $N_m = N$ (we assume here, of course, that a minimum of one turn is possible). Thus, we can define the maximum frequency of operation as

$$\omega_m = \frac{v}{2\ell N} \tag{20}$$

with the constraint that $N = N_m$.

Next, we can assume that $R_L + R_c$ is some multiple of R_i; thus

$$R_L + R_c = \alpha R_i . \tag{21}$$

Then, using the definition of R_i (Eq. 3) and the condition for self-excitation (Eq. 13), we obtain

$$N = \frac{1+\alpha}{\mu_o \sigma \ell v} . \tag{22}$$

Note that the denominator of this expression is a magnetic Reynolds number based on

the length of a pair of electrodes.

Substitution of Eq. 22 in Eq. 20 yields

$$\omega_m = \frac{\mu_o \sigma v^2}{2(1+\alpha)} . \tag{23}$$

This result shows that the maximum frequency of operation depends on the conductivity σ, velocity v, and degree of loading α, and is independent of the size of the device.

To obtain some idea of the conditions that must be satisfied with an ionized gas for ac power generation of this type, we can use Eq. 23 to calculate values. Assuming a frequency of 60 cps, we can rewrite Eq. 23 as

$$\frac{\sigma v^2}{1 + \alpha} = 6 \times 10^8 .$$

Values of α, σ, and v that satisfy this equation are given in Table VIII-I.

Table VIII-I. Velocity, conductivity, and loading factor for operation at 60 cps.

loading factor α	0	0.5	1.0	2.0
(v m/sec)		(σ mhos/meter)		
1000	600	900	1200	1800
1500	270	400	530	800
2000	150	230	300	450
2500	96	144	190	290
3000	67	100	130	200
3500	49	74	100	150
4000	37	55	75	110

It is apparent from the numbers in Table VIII-I that there is a chance of using this type of generator with combustion gases and with gases having increased conductivity that is due to nonequilibrium effects. At a given velocity and loading factor the required conductivity varies linearly with frequency. Thus the device will work better at frequencies below 60 cps. For gases at combustion temperatures, high-frequency operation (such as 400-1000 cps) does not appear possible because of the high velocities and conductivities required.

The data of Table VIII-I can be used with an assumed length in Eq. 22 to find the number of turns required. To show that the number of turns is reasonable, assume ℓ = 1 meter and use α = 1, v = 3000 m/sec, σ = 130 mhos/meter from Table VIII-I to find N = 4 turns; this value is certainly reasonable for constructing such a device. The

other conditions of Table VIII-I will yield numbers of turns having the same order of magnitude.

3. Segmented Electrodes and Tensor Conductivity

It appears from the numbers mentioned in the preceding section that the number of turns per field coil may be small. For a large generator, the field conductors in such a system may be so large that eddy currents become a problem. Moreover, if the gas has tensor conductivity, the solid electrodes will short out the Hall electric fields and degrade performance.

Both of these deleterious effects can be reduced by using segmented electrodes. The construction for two electrode segments per generator section is illustrated in Fig. VIII-4. The essence of this arrangement is that each electrode pair is connected to a circuit exactly like that for solid electrodes in Fig. VIII-3. The circuit for each

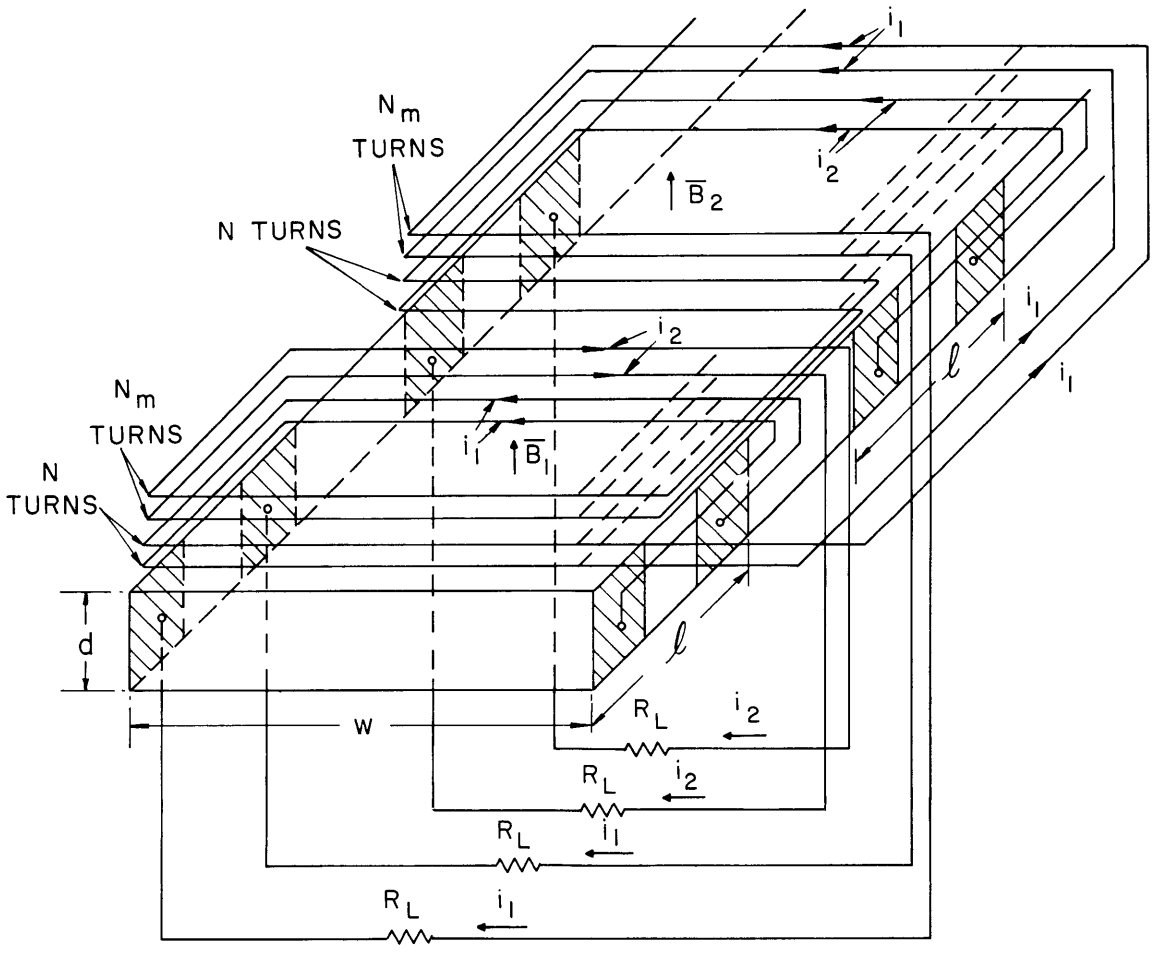

Fig. VIII-4. Configuration for use with segmented electrodes.

electrode pair is electrically insulated from all other circuits. If many electrode pairs are used, the power will probably be extracted by inductive coupling to magnetic fields B_1 and B_2, or by replacing R_L with a transformer winding. In any case, the generation of ac power with segmented electrodes does not create the problem of having many insulated loads that a dc generator does.

For the analysis assume that there are n electrode segments per generator (of length ℓ) and that the coils span a distance ℓ in the flow direction. If each pair of electrodes is assumed to carry the same current as other segments in the same generator section, then for the flux densities B_1 and B_2 (see Eqs. 1 and 2) we can write

$$B_1 = \frac{nN\mu_o}{d} i_1 - \frac{nN_m\mu_o}{d} i_2 \tag{24}$$

$$B_2 = \frac{nN\mu_o}{d} i_2 + \frac{nN_m\mu_o}{d} i_1 . \tag{25}$$

Assuming a one-dimensional model, the internal resistance R_i' associated with a pair of electrodes (see Eq. 3) is

$$R_i' = nR_i = \frac{nw}{\ell d\sigma} . \tag{26}$$

The equations for single electrode pairs in the two generator sections (see Eqs. 4 and 5) are

$$vwB_1 = R'i_1 + N\ell w \frac{dB_1}{dt} + N_m \ell w \frac{dB_2}{dt} \tag{27}$$

$$vwB_2 = R'i_2 + N\ell w \frac{dB_2}{dt} - N_m \ell w \frac{dB_1}{dt}, \tag{28}$$

where $R' = R_L + R_i' + R_c$ is the total series resistance in one electrode-pair circuit.

Substituting Eqs. 24 and 25 in Eqs. 27 and 28 and simplifying (see Eqs. 6 and 7) yields

$$G_n i_1 - G_{mn} i_2 = R'i_1 + L_n \frac{di_1}{dt} \tag{29}$$

$$G_n i_2 + G_{mn} i_1 = R'i_2 + L_n \frac{di_2}{dt} . \tag{30}$$

The parameters G_n, G_{mn}, and L_n are defined as

$$G_n = \frac{nN\mu_o vw}{d} \tag{31}$$

$$G_{mn} = \frac{nN_m\mu_o vw}{d} \tag{32}$$

$$L_n = \frac{n\mu_o \ell w}{d}\left(N^2+N_m^2\right) \tag{33}$$

For this system self-excitation is achieved when the parameters are adjusted to satisfy the condition

$$G_n = R'. \tag{34}$$

With this condition satisfied, the frequency of steady-state operation is

$$\omega = \frac{G_{mn}}{L_n}. \tag{35}$$

By using the definitions of Eqs. 32 and 33, the frequency can be expressed as

$$\omega = \frac{vN_m}{\ell\left(N^2+N_m^2\right)}. \tag{36}$$

This is exactly the same as Eq. 19 for the system with solid electrodes.

The maximum frequency occurs when $N_m = N$, and is

$$\omega_m = \frac{v}{2\ell N}. \tag{37}$$

Defining the parameter a as

$$R_L + R_c = aR_i' \tag{38}$$

we can use the self-excitation condition, Eq. 34, with Eq. 26 to obtain

$$N = \frac{1+a}{\mu_o \sigma \ell v}. \tag{39}$$

Note that the results of Eqs. 36, 37, and 39 are independent of the number of electrode segments and are the same as Eqs. 19, 20, and 22 for the system with solid electrodes. Thus, all of the discussion of limiting parameters in the preceding section holds also for the case of segmented electrodes. The only effect of segmenting the electrodes is to require a number of windings that is equal to the number of electrodes, each winding having the same number of turns as required by the machine with solid electrodes. Each winding carries a fraction 1/n of the total current supplied by a generator section; consequently, the volume of field conductor is independent of the number of electrode segments.

4. Discussion

The generators discussed in this report on an idealized basis indicate the possibility of their being applicable to systems in which ionized gases are used at temperatures

that are characteristic of combustion processes. Their advantage is that they generate alternating current directly and use only magnetic fields for energy storage.

The theory assumes incompressible flow. The basic mechanism still occurs in compressible flow, the velocity being the average flow velocity of the gas. There will be compressibility effects that need to be evaluated and they may even augment the conversion process.

The generators analyzed here are two-phase machines. By a simple extension of the concepts we can devise an n-phase machine by having n separate sets of electrodes and n sets of magnet coils along the channel. A coupling coil is required in each set for current from every other set of electrodes. No matter how many phases a machine may have, it can be reduced to an equivalent two-phase machine for analysis. Thus the present analysis is complete for a balanced n-phase machine.

H. H. Woodson

References

1. H. H. Woodson, Magnetohydrodynamic A-C Power Generation, Proc. AIEE Pacific Energy Conversion Conference, San Francisco, California, August 1962.

C. ELECTROHYDRODYNAMIC WAVES IN ROTATIONAL SYSTEMS

1. Introduction

Efforts to achieve a stable magnetohydrodynamic containment have led some investigators to consider the effect of rotation. From everyday experience, one would suspect that rotational acceleration, just as the acceleration of gravity, could be responsible for stabilizing or unstabilizing a system, the choice depending on the configuration. Common examples are the gravitational or Taylor instability, produced by gravity on a top-heavy fluid interface[1] or the stabilizing influence of gravity in a situation in which a perpendicular electric field is responsible for a surface instability.[2]

However, it is well known that rotational motion is considerably more involved than this. In addition to the centrifugal forces experienced in pure rotation, particles that are in motion with respect to a rotating frame respond to a Coriolis acceleration, which results in a mode splitting that has been well known since the last century in conjunction with ordinary gravity waves,[3] but has been studied in detail only recently.[4]

This report is a study of the three types of surface interactions in circular cylindrical geometry. The surface not only has an equilibrium curvature, but is also subject to accelerations associated with a steady rigid-body equilibrium rotation.

There are two reasons for wishing to study systems of this type. The great interest in stabilizing MH systems in connection with the thermonuclear program has already

been mentioned. The antiduality of MH and EH systems, which has been pointed out elsewhere,[5] should serve to show that study of the EH-If system can lead to a better understanding of the MH counterpart. An experimental investigation of the EH problem is possible, whereas the MH system can be considered experimentally only with great difficulty. In the second place, the study of cylindrical field coupled

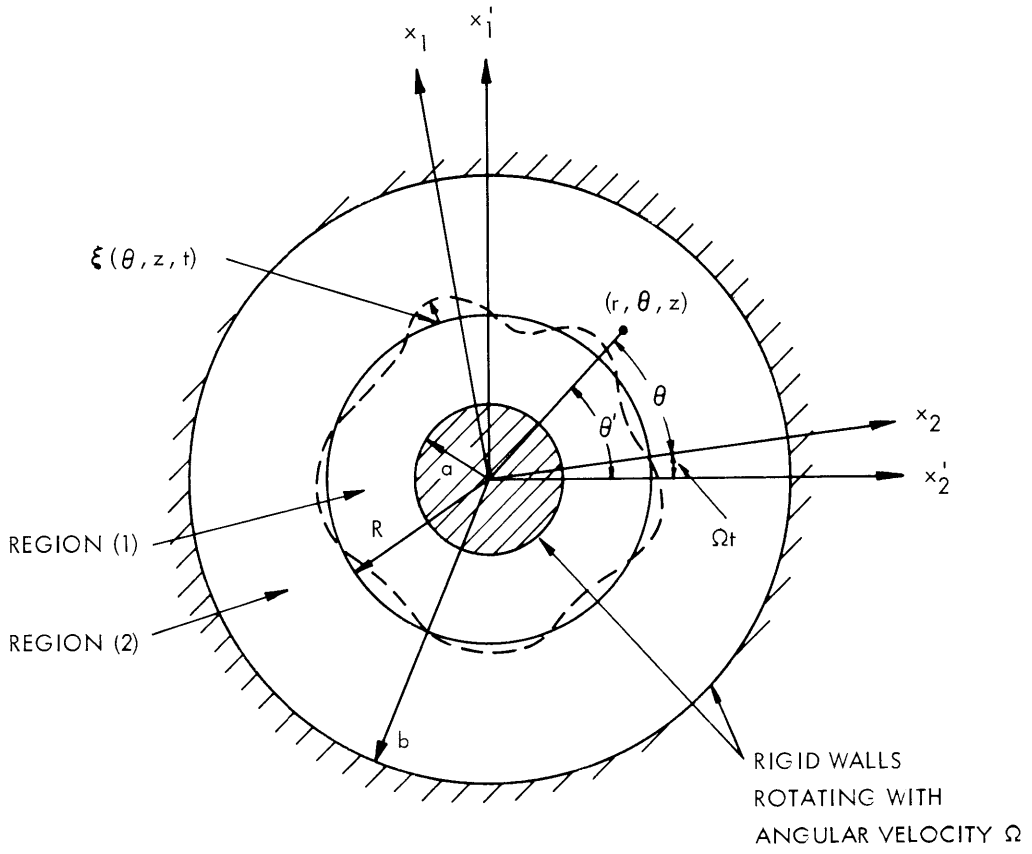

Fig. VIII-5. Cross section of rotating structure showing dimensions.

systems has always been of primary interest in spite of the fact that it is very difficult to achieve, experimentally, an equilibrium cylindrical geometry that approaches the idealization of a cylinder. For example, a jet in free fall changes in radius radically over a short distance unless the velocity is made high enough to produce turbulence. In fact, the very velocity of the jet is not a trivial addition to the dynamics, as has been shown in dealing with the convective systems.[6] In contrast, here we shall remove the effect of rotational convection by considering all interactions, both theoretically and experimentally, in the rotating frame.

2. Description of Problems

The mechanical configuration that will be considered here is shown in Fig. VIII-5. The region between two coaxial rigid circular cylinders is filled with two inviscid, incompressible nonmiscible fluids in such a way that they form an equilibrium interface at a radius R. The cross section is assumed to remain constant. The complete assembly is then assumed to rotate with an equilibrium rotational velocity Ω. It is possible to produce such a configuration by filling a cylinder with two fluids and rotating the cylinder fast enough to centrifugally drive the heavier fluid to the outside. The essentially rigid body rotation that results depends on the centrifugal acceleration being large compared with the acceleration of gravity. Hence, this last acceleration will be ignored in this analysis.

Although it is not usual to view them as such, problems of this kind are characterized by a discrete set of possible transverse modes so that they comprise a type of surface resonator.[7] This is most apparent if there is no axial dependence of the modes considered. In the experiments described in this report, the technique used to verify the theoretical considerations will take advantage of this fact. In any case, an experiment must involve a finite structure so that the axial modes will also be selected from a discrete set of wave numbers.

Here, both EH-I and EH-II interactions will be considered. The type EH-1 interaction is produced by an electric field that, in general, is in the radial direction. The EH-Ip is produced by equipotentials on the inner and outer cylinders because the region between would be filled with dielectric. However, in the EH-If interaction either the inner or outer cylinder can form one of the equipotentials, while the other might be formed by the interface. For the EH-II interaction, the inner and outer cylinders must be dielectrics, with the electric field imposed by parallel plates that are perpendicular to the z-axis. The types of velocity and electric fields to be considered are given by

$$V' = V_1'\bar{a}_1 + (\Omega r + V_2')\,\bar{a}_2 + V_3'\bar{a}_3 \tag{1}$$

$$\left.\begin{array}{l} \text{EH-If} \\ \text{EH-Ip} \end{array}\right\} \bar{E} = \left(\frac{v}{r} + e_1\right)\bar{a}_1 + e_2\bar{a}_2 + e_3\bar{a}_3$$

$$\left.\text{EH-II}\right\} \bar{E} = e_1\bar{a}_1 + e_2\bar{a}_2 + (E_o + e_3)\,\bar{a}_3 \Bigg\} \tag{2}$$

3. E-H Equations of Motion

The EH bulk equations will be taken as

$$\nabla \cdot \bar{V}' = 0 \tag{3}$$

$$\rho \frac{D\bar{V}'}{Dt} + \nabla p' = 0 \tag{4}$$

$$\nabla \times \overline{E} = 0 \tag{5}$$

$$\nabla \cdot \epsilon \overline{E} = 0, \tag{6}$$

where p' is the total pressure given by

$$p' = P + \frac{1}{2}\epsilon E^2.$$

The primes denote quantities evaluated in the rest frame. The velocities of interest are not large enough to require any distinction between frames for the electric fields.

It is apparent that the mechanics would be considerably simplified by viewing the motion from the rotating frame. For this reason, Eqs. 3 and 4 will now be transformed to the rotating frame. This is accomplished by the transformation

$$\begin{aligned} r &= r' & V_1' &= V_1 \\ \theta &= \theta' - \Omega t & V_2' &= V_2 + \Omega r \\ z &= z' & p' &= p_o + p \\ t &= t' \end{aligned} \tag{7}$$

If only linear terms are retained, the momentum and continuity equations require

$$p_o = \frac{1}{2}\rho\Omega^2 r^2 + \text{constant} \tag{8}$$

$$\rho\left[\frac{\partial V_1}{\partial t} - 2\Omega V_2\right] + \frac{\partial p}{\partial r} = 0 \tag{9}$$

$$\rho\left[\frac{\partial V_2}{\partial t} + 2\Omega V_1\right] + \frac{1}{r}\frac{\partial p}{\partial \theta} = 0 \tag{10}$$

$$\rho\left[\frac{\partial V_3}{\partial t}\right] + \frac{\partial p}{\partial z} = 0 \tag{11}$$

$$\frac{1}{r}\frac{\partial r V_1}{\partial r} + \frac{1}{r}\frac{\partial V_2}{\partial \theta} + \frac{\partial V_3}{\partial z} = 0. \tag{12}$$

The terms in these equations are those that would be observed by a rotating observer. The usual techniques are now used to handle these equations. The total pressure is used as a potential for deriving the other mechanical variables, while the axial electric field is used to determine the remaining field components.

Because of the cylindrical geometry, the eigenvalues satisfying the axial boundary conditions can be chosen from those given by the assumed solution,

$$p = \hat{p}\, e^{j(\omega t + m\theta + kz)}. \tag{13}$$

Here, ω is the frequency as viewed in the moving frame. In all present considerations care will be taken to excite and measure all frequencies in the moving frame.

If the surface of the interface is to be continuous azimuthally, the eigenvalue m must have integer values. The wave number k will be determined in the usual way from the boundary conditions in the axial direction.

The assumed solution reduces the bulk equations of motion given by Eqs. 5, 6, and 9-12 to a pair of ordinary differential equations that define all of the remaining functions.

$$r^2 \frac{d^2\hat{p}}{dr^2} + r \frac{d\hat{p}}{dr} - \hat{p}[m^2+r^2k^2\Delta^2] = 0, \tag{14}$$

where

$$\Delta^2 = \left[1 - \frac{4\Omega^2}{\omega^2}\right]$$

$$\frac{1}{r}\frac{dr}{dr}\left(\frac{d\hat{e}_3}{dr}\right) - \hat{e}_3\left[\frac{m^2}{r^2} + k^2\right] = 0. \tag{15}$$

Here, in terms of $\hat{p}$ and $\hat{e}_3$, the remaining functions are

$$\hat{V}_1 = \frac{j}{\rho\omega\Delta^2}\frac{d\hat{p}}{dr} + \frac{2jm\Omega}{\Delta^2\rho\omega^2}\left(\frac{\hat{p}}{r}\right) \tag{16}$$

$$\hat{V}_2 = \frac{-m}{\rho\omega\Delta^2}\left(\frac{\hat{p}}{r}\right) - \frac{2\Omega}{\Delta^2\rho\omega^2}\frac{d\hat{p}}{dr} \tag{17}$$

$$\hat{V}_3 = \frac{-k\hat{p}}{\rho\omega} \tag{18}$$

$$\hat{e}_2 = \frac{m}{k}\left(\frac{\hat{e}_3}{r}\right) \tag{19}$$

$$\hat{e}_1 = \frac{-j}{k}\frac{d\hat{e}_3}{dr}. \tag{20}$$

It is convenient to use as solutions to Eqs. 14 and 15 the Bessel function of first kind and the Hankel function of first kind.

$$\hat{p} = A_1 J_m(jk\Delta r) + A_2 H_m(jk\Delta r) \tag{21}$$

$$\hat{e}_3 = C_1 J_m(jkr) + C_2 H_m(jkr). \tag{22}$$

However, we note the important fact that the arguments of these functions as they occur in all of the mechanical variables depend on both the frequency ω and the

wave number k. This is the salient complication of the rotation.

The surface dynamics are represented in terms of the unit normal, n, directed in the positive r direction in equilibrium, and the surface displacement $\xi(\theta, z, t)$ from an equilibrium position R.

$$\frac{D}{Dt}\left[r-(\xi(\theta, z, t)+R)\right] = 0. \tag{23}$$

Remember that ξ is the surface perturbation as viewed in the fixed frame. Hence, Eq. 21 must be transformed to the rotating frame in which it takes on the expected nonconvective form

$$\hat{\xi} = -\frac{j\hat{V}_1}{\omega}. \tag{24}$$

The normal vector does not depend on rates of change with respect to time, and is therefore unaffected by the transformation to the rotating frame of reference. Hence

$$\left.\begin{aligned} \hat{n}_2 &= \frac{-m}{R\omega}\hat{V}_1 \\ \hat{n}_3 &= \frac{-k}{\omega}\hat{V}_1 \end{aligned}\right\}. \tag{25}$$

The boundary conditions are given here for convenience. They are of the same form as those used in conjunction with variables defined in the inertial frame because the transformation of all of the variables involved in the boundary conditions (see Eq. 7) is one to one. Hence, the definition of the interface and the conservation of momentum at the interface require that

$$\bar{n} \cdot \left[\bar{V}^{(2)}-\bar{V}^{(1)}\right] = 0 \tag{26}$$

$$n_\alpha T\left(\frac{1}{R} - \frac{1}{R^2}\left(\xi + \frac{\partial^2\xi}{\partial\theta^2}\right) - \frac{\partial^2\xi}{\partial z^2}\right) - n_\beta\left[T^{(2)}_{\alpha\beta}-T^{(1)}_{\alpha\beta}\right] = 0, \tag{27}$$

where T is the surface tension, and $T_{\alpha\beta}$ is the total stress tensor given by

$$T_{\alpha\beta} = \epsilon E_\alpha E_\beta - \delta_{\alpha\beta}\left[\frac{\epsilon E_\gamma E_\gamma}{2} + p\right].$$

Also, the tangential component of the electric field must be continuous at the interface.

$$n \times \left[\bar{E}^{(2)}-\bar{E}^{(1)}\right] = 0. \tag{28}$$

If there is no free charge on the interface, a type I interaction requires the use of the additional condition

$$\bar{n} \cdot \left[\epsilon^{(2)}\bar{E}^{(2)}-\epsilon^{(1)}\bar{E}^{(1)}\right] = 0. \tag{29}$$

At r = a, b, the normal velocity must vanish because of the condition imposed by a rigid boundary. In the EH-II interaction it is assumed that these boundaries are composed of a dielectric material so that it is possible to support an axial electric field that is uniform in the unperturbed state. The walls are assumed to have the same dielectric properties as the adjacent fluid dielectric, so that there is no polarization charge or Korteweg current on the rigid boundaries. On the other hand, the type I interactions are assumed to result from equipotentials at r = a, b; and this requires that $e_3 = 0$ there.

4. Dispersion Equations

The technique of finding the dispersion equations that are consistent with perturbations of the form of Eq. 13 is now straightforward. Equations 16-20, 24, and 25 make it possible to evaluate all of the dependent variables in terms of the solutions given by Eqs. 21 and 22, that is, in terms of eight constants, $A_1^{(1)}$ $A_2^{(1)}$, $C_1^{(1)}$ $C_2^{(1)}$, $A_1^{(2)}$ $A_2^{(2)}$, $C_1^{(2)}$ $C_2^{(2)}$. (The superscripts denote the region in which the variable is to be evaluated.)

The dispersion relation for each of the problems is the compatibility condition of these eight constants in the equations resulting when the solutions are substituted in the boundary conditions of Eqs. 26-29.

The cylindrical geometry poses the complication of a radial dependence for the equilibrium pressure field; and in the type I interactions, a radial dependence for the equilibrium electric fields. Hence, in this linear analysis, these respective fields must be written in the form

$$P = \text{constant} + \frac{1}{2}\rho\Omega^2(R+\xi)^2 + p(r, \theta, z, t)$$

$$\approx \text{constant} + \frac{1}{2}\rho\Omega^2(R^2+2R\xi) + p(r, \theta, z, t) \tag{30}$$

$$E_1 = \frac{V}{(R+\xi)} + e_1 = \frac{V}{R} - \frac{V}{R^2}\xi + e_1. \tag{31}$$

Investigation shows that for the EH-If interaction, Eqs. 26-29 are linear combinations of Eqs. 26, $(27)_1$, $(27)_3$, $(28)_2$ and the condition that $v_1 = 0$ at r = a, b. One of these equations ceases to be independent in the limit where there is no free charge on the interface. In this case (the EH-Ip interaction) Eq. $(27)_3$ is replaced by Eq. 29.

The EH-II interaction is defined by Eqs. 26, $(27)_1$, $(27)_3$, 28, and the condition that $v_1 = 0$ at r = a, b. It is assumed that all electromagnetic perturbation fields are finite at infinity and at the origin. This last condition replaces two equations, in that it requires $C_1^{(2)} = C_2^{(1)} = 0$. The dispersion equations for each of the three problems can be summarized as follows:

$$\omega^2 = \frac{T}{R^2\rho_{eq}}\{(kR)^2-(1-m^2)+F+G\}, \tag{32}$$

where

$$F = \frac{R^3\Omega^2}{T}\left(\rho^{(2)}-\rho^{(1)}\right)$$

$$\rho_{eq} = \Delta\left[\rho^{(1)}P_m(jk\Delta a, jk\Delta R)-\rho^{(2)}P_m(jk\Delta b, jk\Delta R)\right]$$

$$P_m(x, y) = \frac{1}{jkR}\left[\frac{J_m(y)\,L_m(x) - Q_m(x)\,H_m(y)}{L_m(x)\,Q_m(y) - Q_m(x)\,L_m(y)}\right]$$

$$Q_m(x) = J'_m(x) + \frac{2m\Omega}{\omega}\,\frac{J_m(x)}{x}$$

$$L_m(x) = H'_m(x) + \frac{2m\Omega}{\omega}\,\frac{H_m(x)}{x}$$

$$S_m(kR, kb) = jkR\left\{\frac{H'_m(jkR)\,J_m(jkb) - H_m(jkb)\,J'_m(jkR)}{H_m(jkR)\,J_m(jkb) - J_m(jkR)\,H_m(jkb)}\right\}$$

$$T_m(kR, ka) = jkR\left[\frac{J'_m(jkR)\,H_m(jka) - J_m(jka)\,H'_m(jkR)}{J_m(jkR)\,H_m(jka) - J_m(jka)\,H_m(jkR)}\right]$$

$$\Delta = \sqrt{1 - \frac{4\Omega^2}{\omega^2}}$$

for all of the problems, but G depends on the type of interaction that is considered.

EH-If

$$G = \Gamma^{(2)}[S_m(kR, kb)+1] - \Gamma^{(1)}[T_m(kR, ka)+1]$$

$$\Gamma = \frac{v^2\epsilon}{RT}\,.$$

EH-Ip

$$G = \frac{1}{RT}\left\{\frac{v^{(1)}\,v^{(2)}\left(\epsilon^{(2)}-\epsilon^{(1)}\right)^2}{\dfrac{\epsilon^{(1)}}{S_m(kR, kb)} - \dfrac{\epsilon^{(2)}}{T_m(kR, ka)}} + \epsilon^{(2)}\left(v^{(2)}\right)^2 - \epsilon^{(1)}\left(v^{(1)}\right)^2\right\}.$$

EH-II

$$G = \frac{\left(\epsilon^{(2)}-\epsilon^{(1)}\right)(Rk)^2\, E_o^2 R}{T\left[\epsilon^{(1)}(jkR)\,\frac{J'_m(jkR)}{J_m(jkR)} - \epsilon^{(2)}(jkR)\,\frac{H'_m(jkR)}{H_m(jkR)}\right]}.$$

If modes of motion are considered that have no z dependence, then the dispersion equations take a simple and convenient form that is quadratic in the frequency ω. To show this, it is recognized that as $k \to 0$ (or as perturbations in the axial direction assume an infinite wave length),

$$T_m(kR, ka) \to m\left[\frac{\left(\frac{R}{a}\right)^{2m}+1}{\left(\frac{R}{a}\right)^{2m}-1}\right] \tag{33}$$

$$S_m(kR, kb) \to m\left[\frac{\left(\frac{b}{R}\right)^{2m}+1}{\left(\frac{b}{R}\right)^{2m}-1}\right]$$

$$P_m(x, y) \to \frac{1}{m\Delta}\left[\frac{\left(1+\frac{2\Omega}{\omega}\right)+\left(\frac{y}{x}\right)^{2m}\left(1-\frac{2\Omega}{\omega}\right)}{\left(\frac{y}{x}\right)^{2m}-1}\right]$$

and the dispersion equations become

$$A\left(\frac{\omega}{\Omega}\right)^2 + 2B\left(\frac{\omega}{\Omega}\right) + C + (1-m^2) - F = 0, \tag{34}$$

where

$$A = \frac{F}{m\left(\rho^{(2)}-\rho^{(1)}\right)}\left\{\left[\frac{\left(\frac{R}{a}\right)^{2m}+1}{\left(\frac{R}{a}\right)^{2m}-1}\right]\rho^{(1)} - \left[\frac{\left(\frac{R}{b}\right)^{2m}+1}{\left(\frac{R}{b}\right)^{2m}-1}\right]\rho^{(2)}\right\}$$

$$B = \left(\frac{F}{m}\right).$$

EH-If

$$C = \left(\Gamma^{(1)}-\Gamma^{(2)}\right) + m\left[\Gamma^{(2)}\left[\frac{\left(\frac{b}{R}\right)^{2m}+1}{\left(\frac{b}{R}\right)^{2m}-1}\right] + \Gamma^{(1)}\left[\frac{\left(\frac{R}{a}\right)^{2m}+1}{\left(\frac{R}{a}\right)^{2m}-1}\right]\right].$$

EH-Ip

$$C = \left(\Gamma^{(1)}-\Gamma^{(2)}\right) - \frac{m^2 v^{(2)} v^{(1)}\left(\epsilon^{(1)}-\epsilon^{(2)}\right)^2}{RT\left[\epsilon^{(1)}\frac{\left(1-\left(\frac{R}{b}\right)^{2m}\right)}{\left(1+\left(\frac{R}{b}\right)^{2m}\right)} + \epsilon^{(2)}\frac{\left(1-\left(\frac{a}{R}\right)^{2m}\right)}{\left(1+\left(\frac{a}{R}\right)^{2m}\right)}\right]}.$$

EH-II

$$C = 0.$$

Note that for a given mode (a given integer value of m) A, B, and C are constants fixed by the physical parameters and the geometry. For each mode, there are two possible frequencies of oscillation. In the limit $\Omega \to 0$, these two values of ω approach the same value. Hence, the effect of the rotation is to split the possible resonant frequencies into disparate pairs. The EH-II waves couple to the electric field only if the direction of propagation is in the direction of the equilibrium electric field.[2] It is therefore not surprising that the electric field has no influence on the resonant frequency of the type II resonator if there is no axial dependence of the surface deformations.

5. Experiment

The EH-If waves discussed in the previous sections are being investigated by using the apparatus shown in Fig. VIII-6. The detailed drawing shows the resonator that is rotated with the frequency Ω. This rotation is provided by a dc motor equipped with a feedback loop for speed control. (The measurement of the resonant frequency ω is sensitive enough to require a speed controlled to four significant figures.) The speed is measured within 1/8 of a revolution with a 10-sec sample time, as shown in Fig. VIII-6. An excitation of the surface waves was provided by torque pulsations from a dc motor with its field excited by a square wave having a repetition rate $\omega/2\pi$. Because the oscillator that generated the square wave operates at 16 times the frequency ω, it is possible to measure the excitation frequency to four places, by using a 10-sec sample time.

The low-frequency m = 1 and m = 2 modes have been measured by using a cylinder of length 8.75 in. with a = 0.5 in., b = 1.867 in. and R = 1.31 in. Although frequency shifts with electric field have been observed (they are small), attention has been confined thus far to attempting to understand the waves without field coupling. Figure VIII-7

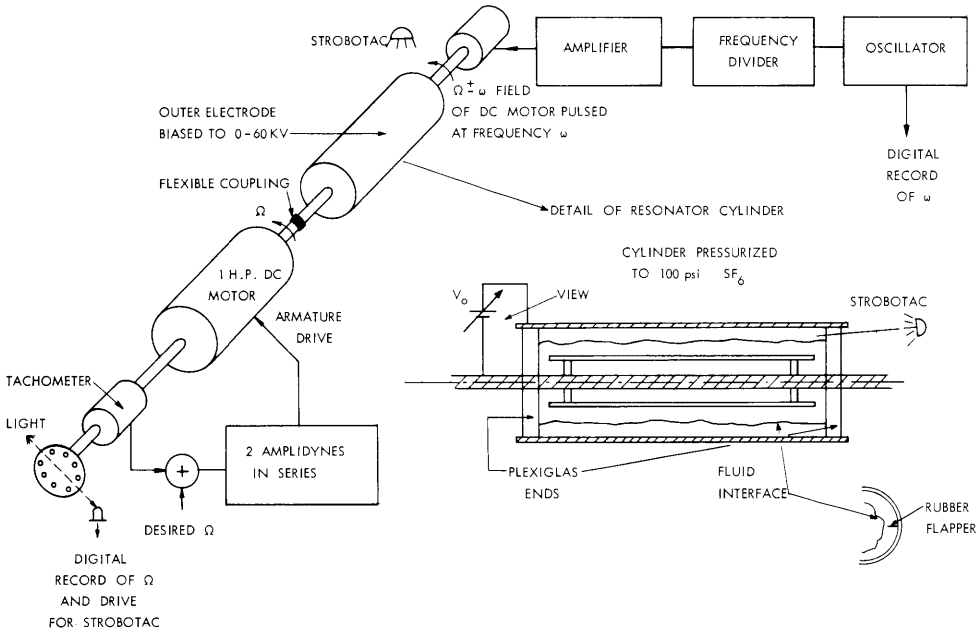

Fig. VIII-6. Experimental arrangement for study of EH surface waves on rotating interface.

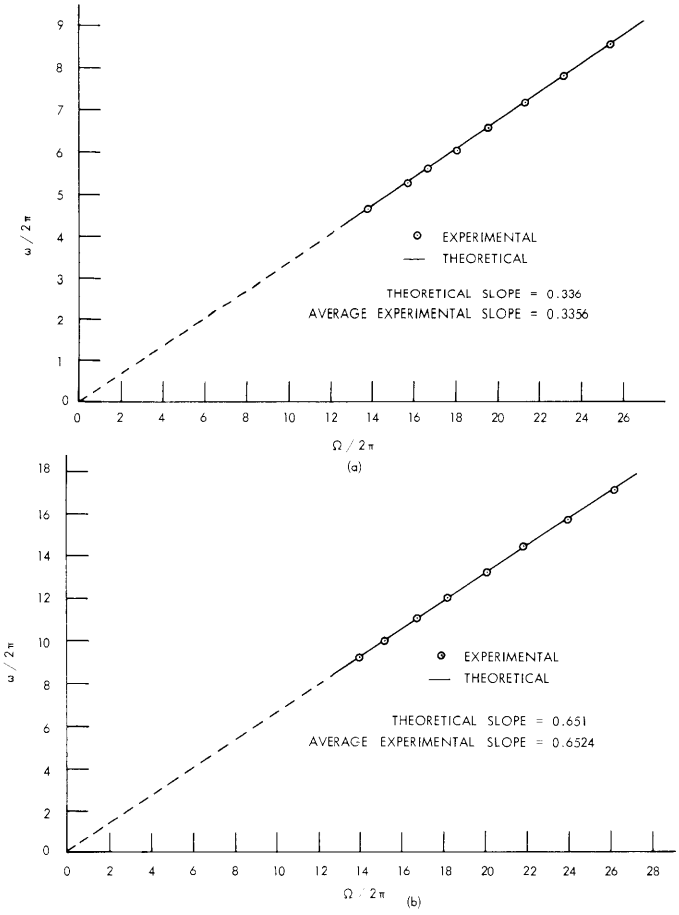

Fig. VIII-7.

(a) Low-frequency m = 1, k = 0 mode (no electric field).
(b) Low-frequency m = 2, k = 0 mode (no electric field).

shows typical data with no electric field. It can be seen that the experiment justifies the mechanical model used (at least for the prediction of the resonant frequency). The solid lines were drawn by using Eq. 34. The surface waves are excited on the interface of the fluid by a thin rubber "flapper" that is attached to the outer wall as shown in Fig. VIII-6. The rotational pulsations of the cylinder then set the fluid into a slight motion which is observed under stroboscopic light. An extremely sensitive indication of resonance is given when the resonant motions of the interface are accompanied by no deflection of the flapper. It is at this frequency that the flapper does not inhibit the motion of the fluid, and hence "pull" the resonant frequency.

J. R. Melcher

References

1. S. Chandrasekhar, Hydrodynamic and Hydromagnetic Stability (Oxford University Press, London, 1961), p. 428.

2. J. R. Melcher, Electrohydrodynamic and magnetohydrodynamic surface waves and instabilities, Phys. Fluids 4, 11 (1961).

3. H. Lamb, Hydrodynamics (Dover Publications, Inc., New York, 1932), p. 307.

4. S. Chandrasekhar, op. cit., p. 284.

5. J. R. Melcher, Field-Coupled Surface Waves (unpublished).

6. J. R. Melcher, Electrohydrodynamic surface resonators, Phys. Fluids 5, 9 (1962).

D. MAGNETOACOUSTIC-WAVE EXPERIMENT

1. Introduction

It has been shown by Haus[1] that it is theoretically possible to use magnetoacoustic waves to convert kinetic power of a flowing plasma to ac electrical power by means of an external, magnetically coupled circuit. In order for this amplifying interaction to occur, the following conditions must be satisfied: (a) the plasma must be flowing through a region of constant applied transverse magnetic field; (b) the flow velocity must be greater than the magnetoacoustic wave velocity, and (c) the plasma electrical conductivity must be sufficiently large to permit the waves to amplify as they propagate.

An experiment has been devised to try to produce a plasma in a system satisfying these conditions. The system is a homopolar device (see Fig. VIII-8) in which a gas is heated and accelerated electrically in a uniform externally applied magnetic field. We are trying to determine whether or not the resulting rotating plasma will satisfy the above-given conditions.

In recent years there has been a growing interest in rotating plasmas for such uses as fast discharge capacitors,[2] arc gas heaters for wind-tunnel or materials studies,[3]

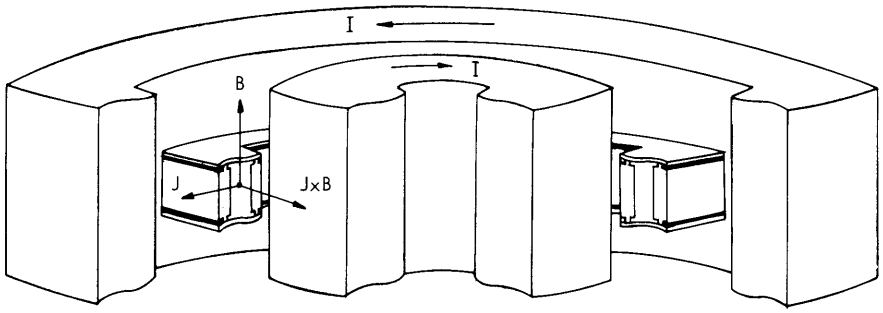

Fig. VIII-8. Homopolar device.

and for basic studies in plasma physics.[4] In each of the cases reported the magnetic field was so large that the flow velocity was less than the magnetoacoustic-wave propagation velocity. Furthermore, there were no attempts to study magnetoacoustic waves. Nevertheless these studies have provided a useful starting point and some theoretical framework for the experiments reported on here. Some initial experiments will be described in which the objective was to produce a plasma satisfying the conditions discussed above.

2. Description of Experiment

The apparatus for the experiment is shown in Fig. VIII-9. The channel (Fig. VIII-10) consists of two concentric circular brass rings. The top and bottom cover plates are either glass or Plexiglas. The inside surfaces of the brass electrodes are notched near the insulating walls and coated with sauereisen, a high-temperature porcelainlike material, in an attempt to confine the plasma away from the insulating walls. The electrode currents are carried by 4 radial arms that join at the axis beneath the electrodes. The chamber is sealed by 4 neoprene O-rings. No external support is required for the cover plates once the chamber is evacuated. The axial magnetic field is produced by two concentric coils connected in series; the field in the region between the coils is uniform within ±5 per cent. Five taps are provided on each coil to vary the amount of inductance from 3-30 mh. The energy for powering the field coils and the plasma is supplied by an 800-μf, 4-kv capacitor bank. The duration of an experiment is 10 msec, or less, depending on the parameters of the system, so that no external cooling is necessary for either the coils or channel. The switching elements used in the experiments are type 5550 ignitrons, which are air-cooled and rated at 12 kv and 20 coulombs for pulse work,[5] or, for example, 20,000 amps for 1 msec. The ignitron igniters are excited by 5C22 hydrogen thyratrons that are fired by delay circuits and pulse-forming networks. See Fig. VIII-11.

The channel is evacuated to approximately 1 μ Hg pressure before each firing and

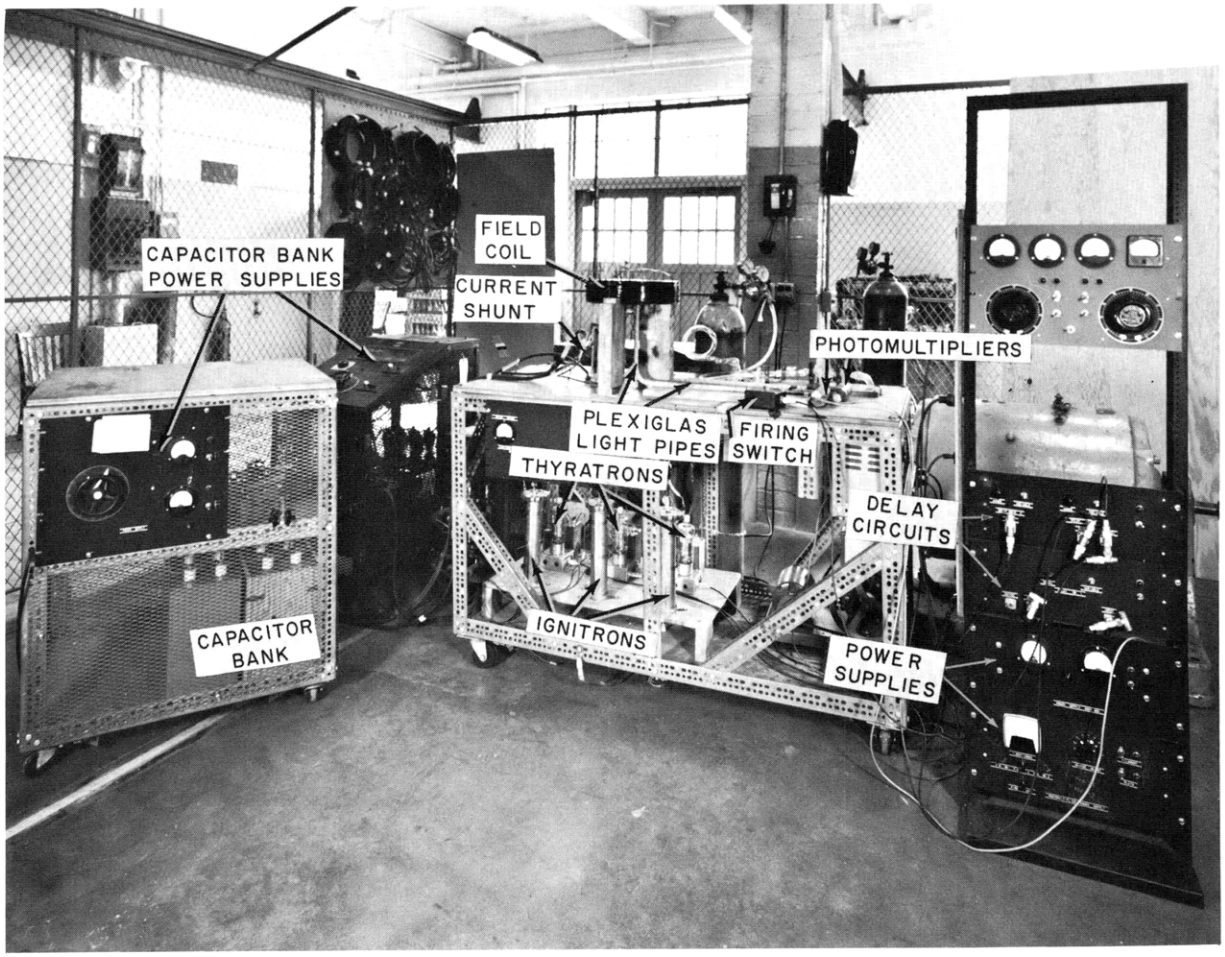

Fig. VIII-9. Rotating-plasma apparatus.

backfilled to the desired pressure with the working fluid. Most of the experiments were performed with helium in the pressure range 0.5-10 mm Hg. At pressures much out of this range it was not possible to break down the gas with the available capacitor bank when an external magnetic field was applied.

Several channel configurations had been used in previous experiments, which formed the basis for the present design. Two circuit configurations have been studied: (a) a series connection in which the field coils are in series with the plasma and (b) separately excited circuits in which the channel and field coils are pulsed from separate capacitor banks. The series arrangement has the advantages that it (a) uses the coil inductance for current limiting, (b) provides a reasonably long discharge time and (c) produces high magnetic fields. A peak discharge current of 1400 amps and magnetic field of 15,000 gauss is possible with a discharge time of 5 msec. At lower field and discharge currents an arc is observed to accelerate azimuthally until a point is reached at which

Fig. VIII-10. Channel with field coils removed.

time the arc suddenly switches mode and becomes diffuse for most of the remainder of the discharge. The current, voltage, and light intensity are illustrated in Fig. VIII-12. The only noted effect of pressure changes in the range 0.5-10 mm Hg was that the plasma was not diffuse as long during the discharge time at the higher pressures. From the

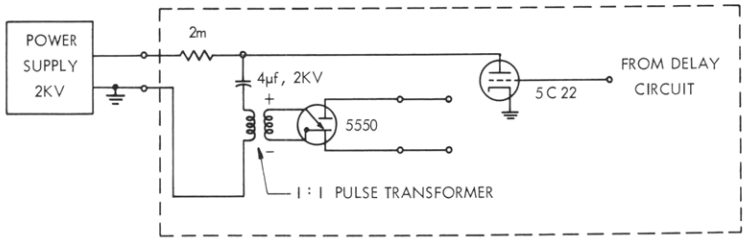

Fig. VIII-11. Typical ignitron firing circuit.

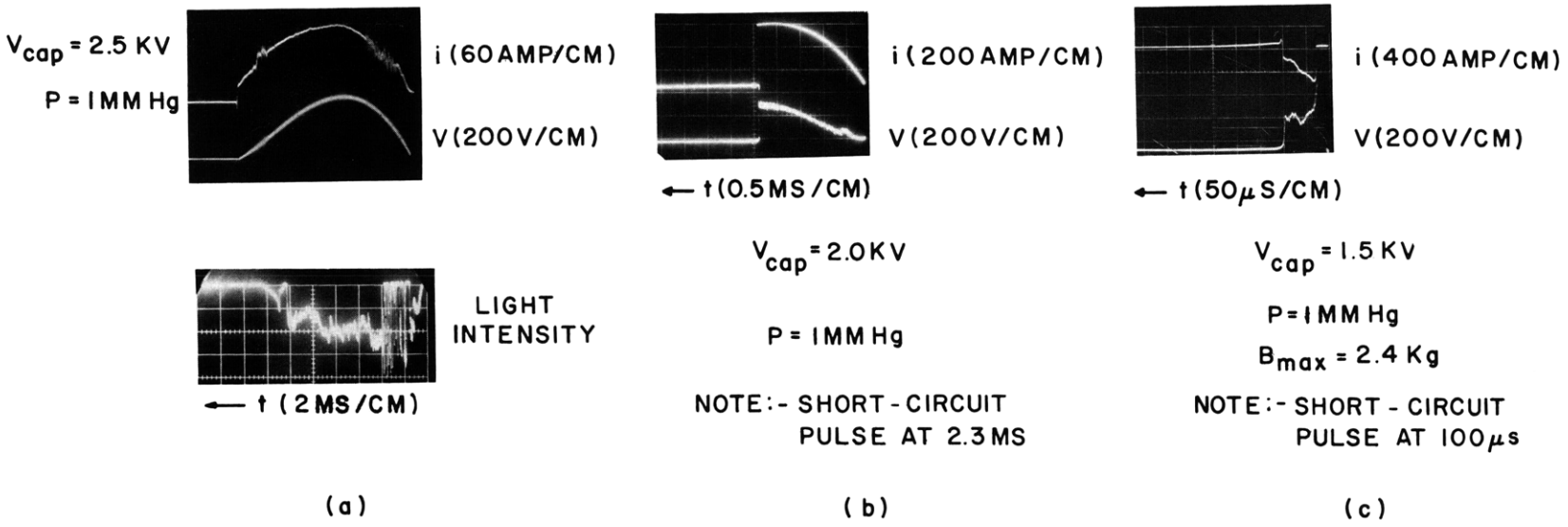

Fig. VIII-12. Waveforms of rotating plasma.

voltage and current traces the voltage is quite nearly proportional to the current. This would be true, for example, if the voltage was produced by a $\vec{v} \times \vec{B}$ back emf if we assume a limiting velocity for the plasma. The velocity corresponding to the values given is of the order of the ionization energy velocity, a result shown by others.[6,7] Attempts to short-circuit the plasma to measure the charge stored in the plasma capacitor, however, did not show any measurable stored charge.

If the inductance of the field coils is reduced, then with a peak field of 6500 gauss and a discharge current of 600 amps, short-circuiting the plasma resulted in the recovery of approximately 100 μcoulomb of charge. This is equivalent to an ionization of 0.1 per cent (or $n_i = 10^{13}$ ions/cc) if it is assumed that the rotational energy of the ions is of the order of the ionization energy. Observations of the light intensity indicate that at the higher currents and magnetic fields the rotating arc phase of the discharge no longer appears.

With the separately excited configuration used and with a current-limiting resistor of 0.6 ohm in the plasma circuit, experiments indicate that the plasma again exhibits capacitive properties (Fig. VIII-12c). In these experiments the magnetic field is first established by part of the capacitor bank and the remainder of the bank is discharged into the channel when the field is maximum.

At the present time we are proceeding with instrumentation to determine conditions experimentally in the rotating plasma. Attempts to launch magnetoacoustic waves in the rotating plasma have been inconclusive.

F. D. Ketterer

References

1. H. A. Haus, J. Appl. Phys. 33, 2161-2172 (1962).

2. O. Anderson, W. Baker, A. Bratenahl, H. Furth, and W. Kunkel, J. Appl. Phys. 30, 188 (1959).

3. R. Mayo and D. Davis, Jr., American Rocket Society Electric Propulsion Conference, Berkeley, California, March 1962.

4. K. Halbach, W. Baker, and R. Layman, Phys. Fluids 5, 1482 (1962).

5. D. B. Hopkins and P. F. Pellissier, UCRL-9968, Lawerence Radiation Laboratory, University of California, Berkeley, Calif., December 11, 1961.

6. H. Alfvén, Res. Modern Phys. 32, 710 (1960).

7. U. V. Fahleson, Phys. Fluids 4, 123 (1961).